

Nanoscale

Accepted Manuscript



This is an *Accepted Manuscript*, which has been through the Royal Society of Chemistry peer review process and has been accepted for publication.

Accepted Manuscripts are published online shortly after acceptance, before technical editing, formatting and proof reading. Using this free service, authors can make their results available to the community, in citable form, before we publish the edited article. We will replace this *Accepted Manuscript* with the edited and formatted *Advance Article* as soon as it is available.

You can find more information about *Accepted Manuscripts* in the [Information for Authors](#).

Please note that technical editing may introduce minor changes to the text and/or graphics, which may alter content. The journal's standard [Terms & Conditions](#) and the [Ethical guidelines](#) still apply. In no event shall the Royal Society of Chemistry be held responsible for any errors or omissions in this *Accepted Manuscript* or any consequences arising from the use of any information it contains.

Full Paper**Facile fabrication of wafer-scale MoS₂ neat films with enhanced third-order nonlinear optical performance**

Xiaoyan Zhang,^a Saifeng Zhang,^a Chunxia Chang,^a Yanyan Feng,^a Yuanxin Li,^a Ningning Dong,^a Kangpeng Wang,^a Long Zhang,^a Werner J. Blau^b and Jun Wang*^a

a Key Laboratory of Materials for High-Power Laser, Shanghai Institute of Optics and Fine Mechanics (SIOM), Chinese Academy of Sciences (CAS), Shanghai 201800, China. E-mail: jwang@siom.ac.cn

b School of Physics and the Centre for Research on Adaptative Nanostructures and Nanodevices (CRANN), Trinity College Dublin, Dublin 2, Ireland

Electronic supplementary information (ESI) available. See Doi: 10.1039/

Abstract

Wafer-scale MoS₂ neat films with controllable thicknesses were successfully fabricated using vacuum filtering from liquid-exfoliated MoS₂ dispersions. The obtained MoS₂ filtered thin films were systematically characterized by UV-Vis spectroscopy, Fourier transform infrared spectroscopy (FTIR), Raman spectroscopy, atomic force microscopy (AFM) and scanning electron microscopy (SEM). It was found that the fabricated scalable MoS₂ films have smooth surface and high optical homogeneity verified by AFM and a collimated 532 nm beam, respectively. We investigated the ultrafast nonlinear optical property (NLO) of the filtered films by open aperture Z-scan method using 515 and 1030 nm femtosecond laser pulses, respectively. Saturable absorption was observed at both 515 and 1030 nm with the figure of merit (FOM) values as $\sim 3.3 \times 10^{-12}$ esu cm and $\sim 3.4 \times 10^{-14}$ esu cm, respectively. The observation of ultrafast NLO performance for the MoS₂ filtered films indicates that the vacuum filtration is a feasible method for fabrication of optical thin films, which can be expanded to fabricate other two-dimensional films from corresponding dispersions. This easy film fabrication technology will greatly enlarge the application of graphene analogous including graphene in photonics devices, especially MoS₂ as saturable absorber.

Keywords: MoS₂ thin film, vacuum filtration, nonlinear optics, saturable absorption, mode-locking

Introduction

Nonlinear optical (NLO) response is an important aspect of light-matter interaction and can play important role in a variety of photonic and optoelectronic applications, especially in those involving high intensity laser beams. Layered MoS₂ semiconductor, a typical graphene analogue, has been reported to have potential applications in the field of photonics and optoelectronics, due to its controllable band gaps from 1.2 to 1.9 eV as well as high carrier mobility and high strength.¹⁻³ Early in 2006, Loh et al. reported the NLO performance of MoS₂ nanotubules in suspensions, which showed good optical limiting behavior for nanosecond laser pulses at 532 and 1064 nm.⁴ Very recently, we reported the ultrafast saturable absorption (SA) behavior of two-dimensional (2D) MoS₂ nanosheets in dispersions under femtosecond laser excitation at 800 nm, which is stronger than that of graphene in dispersions.⁵ Afterwards, the broadband SA performance as well as its mode locking and Q-switching operations for fiber laser or solid laser was reported for layered MoS₂,⁶⁻¹¹ showing potential of few-layer MoS₂ for ultra-short pulse generation. However, most of the works reported, to the best of our knowledge, have been focused on the NLO study of materials in liquid state.¹² Thus, from a practical point of view, fabrication of high quality film state NLO nanomaterials, especially neat thin films, becomes very important and timely. Moreover, fabrication of neat films can afford a chance to study the intrinsic NLO property of the materials in view of the fact that the solvent or polymer effect on the nonlinear performance cannot be preventable.¹³⁻¹⁵ For example, the mode-locking and Q-switching performances of few-layer MoS₂ are expected to

be enhanced in the absence of polymers such as polyvinyl alcohol (PVA) and poly(methyl methacrylate) (PMMA) due to their photoluminescence.

Though micro-mechanical cleavage¹⁶ and chemical vapor deposition (CVD)¹⁷⁻¹⁹ can afford pure and high quality monolayer MoS₂, especial CVD method, it is still hard to realize the synthesis of large-scale thin film samples. Moreover, the reproducibility and controllability of the micro-mechanical cleavage and CVD methods are still very poor except CVD needing high temperature and expensive set up. By contrast, liquid-phase exfoliation method with the exfoliated dispersions containing a large amount of mono- or few-layer flakes is scalable and permitting fabrication of wafer-scale thin films by filtration, showing good prospects in photonic devices.² It should be emphasized that the liquid-phase exfoliation method in combination to vacuum filtration technique would provide an alternative way to readily achieve large-area layered films from the other transition metal dichalcogenides, which the conventional CVD is not able to fabricate yet, such as, selenides and tellurides. Vacuum filtration has been previously used to fabricate graphene or graphene oxide thin films.²⁰⁻²² However, no systematical work has been reported as far as we know on the fabrication of neat MoS₂ thin films from liquid-phase exfoliation dispersions, especial for the optical application purpose.

In this work, we fabricated large-scale MoS₂ optical thin films from the exfoliated MoS₂ dispersions using vacuum filtration, and systematically investigated the effect of pore size of membrane and amounts of MoS₂ flakes in dispersions on the film thicknesses as well as the structure difference between film-state and liquid-state

MoS₂ flakes. Large-scale MoS₂ thin films were fabricated on different substrates with controllable thicknesses by changing the amount of MoS₂ nanosheets in dispersions or membrane pore sizes. In addition, we studied the ultrafast NLO property of the neat layered MoS₂ films. In comparison with MoS₂ dispersions and graphene filtered films, enhanced SA was observed for the MoS₂ thin films under femtosecond pulses at 515 and 1030 nm. The results imply that the facile film fabrication technology, which is more convenient than CVD and pulsed laser deposition (PLD) method,²³ can afford thickness-tunable layered MoS₂ optical thin films for technological applications.

Experimental Section

Materials. MoS₂ powders (< 2 μm, 99%) and sodium cholate (SC) (≥ 99%) were purchased from Sigma-Aldrich. Porous nitrocellulose membranes (Φ = 47 mm) were purchased from Milipore with different pore sizes (Φ_m = 50 nm, 100 nm, and 220 nm). All materials were used as supplied. The water used in this work was double-distilled water. The substrates used such as quartz, glass and silicon were cleaned by sonication in a mixture of acetone and ethanol, ethanol, and then water for 15 min, respectively.

Synthesis of MoS₂ dispersions. Layered MoS₂ dispersions were prepared by liquid-phase exfoliation method using ionic surfactant sodium cholate (SC) as a stabilizer.²⁵ Typically, 2H MoS₂ powder (5 mg mL⁻¹) was dispersed in an aqueous solution of the surfactant SC (0.1 mg mL⁻¹) and sonicated using a horn probe sonic tip (VibraCell CVX; 750 W) with 38% output power for 1 h. The dispersions after standing for 24 h were then centrifuged at 3000 rpm for 90 min to remove

unexfoliated powders. The top 2/3 of the dispersions was collected by pipette. Similarly, the MoS₂ dispersions centrifuged at 1500 and 6000 rpm were prepared in the same conditions.

Fabrication of MoS₂ transferred films. MoS₂ neat films on different substrates (such as quartzs, glass, and silicon) were obtained by vacuum filtration followed by transferring to substrates.²⁰

The dispersions of MoS₂ at 1500 rpm were generally diluted to 1/60 of the original concentration, and the dispersions at 3000 and 6000 rpm were diluted to 1/15 ~ 1/30 of the original concentrations, respectively, with further sonication for 60 min. Typically, the diluted MoS₂ dispersions (for example, 4 mL dispersions at 3000 rpm into 60 mL) were vacuum-filtrated and rinsed in deionized water. Thereafter, the obtained wet membranes with captured 2D MoS₂ were pressed against the cleaned substrate surface with the MoS₂ side in contact with the substrates. The MoS₂ films were allowed to dry and adhere to the substrates at 30 ~ 70 °C under a 1 kg weight for 5 ~ 12 h. Then the weight was removed and the membranes were soaked slowly in acetone for ~ 40 min by three times (30 mL for each time). The films were then rinsed with methanol for 2 ~ 3 times and dried at 60°C for 1 h. By changing the amount or type of the diluted MoS₂ dispersions and types of membranes as well as the substrates, different samples were obtained. In this work, the MoS₂ films were fabricated using MoS₂ dispersions under a centrifugation rate of 3000 rpm with membrane pore size of 100 nm in the absence of other illustrative cases. Graphene films for comparative use were prepared in the same way from the corresponding dispersions treated with a

centrifugation rate of 3000 rpm for 90 min.

Characterizations. The quality of the MoS₂ dispersions was characterized by transmission electron microscopy (TEM) (JEM-2100F, Japan). The absorption spectra of the MoS₂ dispersions and the neat MoS₂ transferred films were measured using a PerkinElmer Lambda 750 instrument in the region of 200~800 nm. To verify the complete dissolution of the cellulose membranes on the MoS₂ films, Fourier transform infrared spectroscopy (FTIR) was recorded using Nicolet 6700 spectrometer (TE Scientific Instruments). Raman spectroscopy for transferred films was carried out using Raman spectrometer (Renishaw inVia) with an Ar laser at 488 nm and the accuracy as 1 cm⁻¹~2cm⁻¹. The surface morphology of the filtered films was characterized by field-emission scanning electron microscopy (FE-SEM) (Auriga, Carl Zeiss) and atomic force microscopy (AFM) (Dimension 3100, Bruker Nano Inc). The highest lateral resolution and vertical resolution for AFM are 0.1 and 0.01 nm, respectively. Optical homogeneity for the filtered films was measured using 532 nm CW lasers with a diameter of ~ 25 mm for expanded spot.

Nonlinear optical Measurements. An open-aperture Z-scan system was used to investigate the NLO property of the transferred MoS₂ films.^{5,24} Total transmittance through the samples as a function of incident intensity was measured while the samples were gradually moved through the focus of a lens along the z-axis. All experiments were performed by using 340 fs laser pulses at 1030 nm and its second harmonic 515 nm with the repetition rate of 1000 Hz and 100 Hz, respectively. The results were fitted by Z-scan theory and the slow saturable absorber model,³²

$$T(L) = T_0 + \frac{T_{\text{FN}}(L) - T_0}{1 - T_0} (T_{\text{max}} - T_0),$$

where $T_0 = e^{-N\sigma_{\text{gs}}L}$, $T_{\text{max}} = e^{-N\sigma_{\text{es}}L}$, L is the sample thickness, T_0 is the transmission in the low pulse intensity limit, T_{max} is the maximal transmission achieved at very high pulse intensities, N is the absorbers density and T_{FN} is the transmission of an “ideal” saturable absorber ($\sigma_{\text{es}} \equiv 0$).

$$T_{\text{FN}} = \frac{1}{\sigma_{\text{gs}}E(0)} \ln\{1 + T_0[e^{\sigma_{\text{gs}}E(0)} - 1]\},$$

where $E(0)$ is the input beam fluence in units of photons per unit area.

Results and discussion

It has been proven that liquid-phase exfoliation is an effective method to prepare 2D MoS₂ dispersions with high quality.^{2,25} Fig. 1 shows the preparation process, absorption spectra and TEM images of the liquid-phase exfoliated MoS₂ dispersions using SC as surfactant. It can be clearly seen from Fig. 1a that centrifugation rate (r) can greatly affect the color of MoS₂ dispersions at the same centrifugation time. Fig. 1b shows the absorption spectra of the corresponding dispersions. Four characteristic peaks expected for 2H-MoS₂ are observed. The peaks between 600 and 700 nm are ascribed to A and B excitonic transitions arising from the K point of the Brillouin zone, and the other two peaks around 420 nm are attributed to C and D excitonic transitions.² It has been reported that the position of A exciton peak can give the information of average thickness of MoS₂ nanosheets, and a smaller average thickness implies a higher percentage of mono- and few-layers out of all nanosheets in dispersion, for there is a thickness distribution for nanosheets in the

liquid-phase exfoliated dispersions.^{2,26} As shown in Fig. 1b, the position of A exciton is at 671.4 (~1.84 eV), 667.7 nm (~1.85 eV) and 665.8 nm (~1.86 eV) for MoS₂ dispersions at 1500, 3000 and 6000 rpm, respectively, which are equivalent to > 10-layer, ~ 8-layer and ~ 5-layer MoS₂, suggesting a large amount of mono- and bilayer MoS₂ for dispersions at 3000 and 6000 rpm. The smaller shift in the absorption resonance for the positions of A and B excitons (inset in Fig. 1b) at higher centrifugation rate suggests larger amount of mono- and bilayer MoS₂ nanosheets in the dispersions, which is in accordance with the fact that direct gap is only weakly sensitive to the confinement effect.^{27,28}

The concentration was calculated to be 0.013 mg·mL⁻¹ for dispersions at a centrifugation rate of 1500 rpm (after subtraction of the scattering background), 0.011 mg·mL⁻¹ for dispersions at 3000 rpm, and 0.005 mg·mL⁻¹ for dispersions at 6000 rpm, using the Lambert–Beer law, $A/l = \alpha C$, where A/l is the absorbance per cell length, α is the extinction coefficient ($\alpha_{672\text{nm}} = 1517 \text{ L}\cdot\text{g}^{-1}\cdot\text{m}^{-1}$), and C is the concentration.²⁵ High-resolution TEM (HRTEM) of MoS₂ nanosheets (Fig. 1c) shows the flakes are of high quality with clear sandwich structure and typical hexagonal symmetry.

The transferred MoS₂ films studied in this work were fabricated from the above MoS₂ dispersions. Fig. 2 shows the film fabrication process and corresponding characterizations. Fig. 2a shows the film fabrication process and the fabricated films on different substrates. In general, when the concentration of the dispersion is constant, changing the volume of the dispersion or the pore size of membrane will

result in the MoS₂ thin films with different thicknesses. Transferred films with different sizes can be obtained by scissoring the justly obtained filtered films, such as 3 mm × 3 mm on quartz substrates with scissoring and $\Phi = 47$ mm on silicon substrates without scissoring (Fig. 2a). During the fabrication process, it is vital to completely remove the filtering membranes to obtain pure MoS₂ films. Fig. 2b shows the FTIR spectra of pure quartz substrate and quartz/MoS₂/membrane films immersed in acetone with different times. Obviously, at shorter immersion times (e.g. 30 s, 60 s), a large amount of organic functional groups from the nitrocellulose membrane exist in the range of 3800 ~ 2400 cm⁻¹ (Fig. 2b). While no vibrational absorption peaks from membrane were observed with a sufficient immersion time in our conditions (~ 3 h) in compared to pure quartz substrates, suggesting that the membranes can be completely removed in our experimental condition. Fig. 2c shows the FE-SEM image of a piece of filtered film on nitrocellulose membrane with pore size of 100 nm from 4 mL of MoS₂ dispersions. It is obviously that almost all membrane surface was covered by MoS₂ flakes with smooth surface (Fig. 2d,e). HRTEM images in Fig. 2f and g demonstrate the few-layer structure of MoS₂ in filtered films, suggesting the layered structure of MoS₂ flakes in dispersions can be reserved in the film state without serious re-aggregation. In addition, the structure and morphologies of MoS₂ filtered thin films and bulk MoS₂ powders were characterized by XRD and SEM (Fig. S1a-d). In compared to the XRD of bulk MoS₂ powders, only a weak diffraction peak at 13.2° corresponding to (002) plane was observed for MoS₂ filtered thin film, suggesting an enlarged interlayer distance of the (002) plane after ultrasonic treatment. SEM image

shows that the fabricated thin film has a porous surface, which is caused by the porous structure of the filter membrane.

The structure differences of MoS₂ nanosheets in dispersions and in solid thin films were further investigated by comparing their absorption and Raman spectra. Fig. 2h-i show the typical absorption and Raman spectra of MoS₂ filtered films and dispersions at 3000 rpm. All the filtered films exhibit the four characteristic exciton absorption peaks of 2H-MoS₂ in the range of 300 ~ 800 nm, showing no obvious difference in compared to the corresponding dispersions (Fig. 2j). The neat films also show the two characteristic Raman peaks with one at around 407 cm⁻¹ attributed to the A_{1g} mode, and the other one at around 382 cm⁻¹ to E_{2g}¹ mode (Fig. 2i). The frequency difference of the two Raman modes is 25.1, 24.9, and 24.8 cm⁻¹ for thin films at 1500, 3000, and 6000 rpm, respectively, which also exhibit no obvious frequency difference from the corresponding dispersions (Fig. 2k).^{29,30} The results suggest that layered structure of MoS₂ flakes in dispersions can be reserved in the film state without serious re-aggregation, verifying the feasibility of the film fabrication technique.

To select a suitable type of membrane for the film fabrication, a series of films was prepared using membranes with different pore sizes. MoS₂ dispersions with 1500 and 6000 rpm were used as examples, considering the larger size differences between the two sorts of dispersions. Fig. 3a shows the photographs of MoS₂ thin films on different pore sizes of membranes before transferring. Obviously, the color of the films becomes paler with the pore size of membranes increasing for both MoS₂ dispersions at 1500 and 6000 rpm. The color differences between films obtained with

membrane pore size of 50 and 100 nm are small, while large color difference occurs when the membrane pore size increases to 220 nm for both dispersions at 1500 and 6000 rpm. The same trend was observed from the absorption spectra. Fig. 3b-c shows the comparative absorption spectra of the corresponding films at 1500 and 6000 rpm, respectively. The film absorbance presents a small decrease with membrane pore size from 50 to 100 nm, and a large decrease with the pore size from 100 to 220 nm at 1500 rpm (Fig. 3b). The large decrease in film absorbance between the two films using membrane pore sizes of 100 and 220 nm suggests a large amount of the flakes passed through the filter membrane with pore size of 220 nm, which in turn indicates that a large amount of the flakes have lateral sizes less than 220 nm. Similarly, the small decrease in film absorbance between the two films with membrane pore size of 100 nm and 50 nm demonstrates most of the flakes were retained on the surface of filter membrane, suggesting that most of the flakes have lateral sizes larger than 50 nm. The results suggest that a large amount of MoS₂ nanosheets in dispersions have lateral sizes in the range of 50 ~ 220 nm, which is in line with our previous work.⁵ The positions of A exciton mainly centered around 1.84 eV for the films at 1500 rpm, corresponding to > 10-layer MoS₂ nanosheets, which is in line with that of the dispersions (inset in Fig. 1b), though a little red shift was observed for both A and B excitonic transitions with increasing membrane pore size from 50 to 220 nm. The same trend was observed for filtered films at 6000 rpm (Fig. 3c). It should be mentioned that the positions of A exciton are equivalent to ~ 8-layer MoS₂ when using membrane pore sizes of 50 and 100 nm, while equivalent to ~ 5-layer MoS₂

when using membrane pore size of 220 nm for the filtered films from dispersions at 6000 rpm. The increased layer number (\sim 8-layer MoS₂) in comparison to the dispersions (\sim 5-layer MoS₂) is probably attributed to part reaggregation of the MoS₂ nanosheets during vacuum filtering process, which is in accordance with the above results (Fig. 2h-i). The results suggest that the lateral sheets size have little effect on the absorbance shift.

Raman spectra were recorded to further study the structure difference among the films fabricated using membranes with different pore sizes. Fig. 3d-e shows the comparative Raman spectra of MoS₂ films with different membrane pore sizes. The two characteristic Raman peaks (A_{1g} mode and E_{2g}¹ mode) were observed. No significant frequency difference in the position of the two Raman modes was seen for films with three different pore sizes of membranes at both 1500 and 6000 rpm, suggesting the membrane pore size has less of an effect on the structure difference in our experimental condition, whereas it can alter the size distribution of MoS₂ nanoflakes to some extent. It should be mentioned that the time needed to make the films from membranes with pore size of 50 nm (\sim 8 min) is almost three times longer than that from membranes with pore size of 100 nm (\sim 3 min) in the process of vacuum filtering in our experimental conditions, while it requires less than 1 min for membranes with pore size of 220 nm. The above results indicate that membranes with pore size of 100 nm would be the best choice for fabrication of the MoS₂ thin films in view of taking less time while intercepting more MoS₂ flakes. The effect of centrifugation rates and membrane pore sizes on the film thicknesses is in line with

the above results (Table S1). To ensure the quality of the films, 1 mL of dispersions at 1500 rpm, and 4 mL at 3000 and 6000 rpm were adopted in the experiment.

Low surface roughness and high optical homogeneity are very important criteria for optical films. Hence, the roughness of the MoS₂ neat films was characterized by atomic force microscopy (AFM). Fig. 3f shows an AFM image of a filtered film on quartz substrate. An average roughness of ~ 10 nm can be observed, indicating the deposited films have a good optical surface. Moreover, it was found that the film thicknesses and the filter membrane pore sizes as well as the centrifugation rates for dispersions have a very little effect on the average surface roughness (Table S2). The optical homogeneity of the films was characterized by a collimated beam from a CW laser light at 532 nm with a diameter of 25 mm. Fig. 3g shows the collimated beam after and before passing through a MoS₂ thin film. No significant scattering and distortion can be seen for the beam after passing through the sample, suggesting the transferred films have high optical homogeneity.

By varying the amount of MoS₂ nanosheets in dispersions, the thicknesses of the films can be easily controlled with a minimal thickness as low as 10 nm. Fig. 4 shows the relationship between film thickness and the amount of MoS₂ nanosheets in dispersions with different centrifugation rates. Obviously, at the same amount of MoS₂ flakes in dispersions, films fabricated from dispersions with a higher centrifugation rate have lower film thickness, which is ascribed to the size distribution difference.³¹

The ultrafast NLO behavior of the MoS₂ neat films was characterized by an

open-aperture Z-scan system under 340 fs laser pulses at 515 and 1030 nm, respectively. Fig. 5a shows the normalized transmission of the MoS₂ films with the film thickness as ~ 90 nm as a function of the input laser intensity, which exhibits broadband absorption saturation at both 515 and 1030 nm. The data in Fig. 5 were fitted with the Z-scan theory and a slow saturable absorber model (see Experimental Section),³² for the excited state decay time (tens of ps) was longer than the pulse duration of 340 fs, referring to a three-level system (Fig. S2).³³⁻³⁵ The NLO fitting parameters are summarized in Table 1 (for a complete data, see Table S3 and S4). Obviously, the nonlinear SA coefficient (α_{SA} , -2.1×10^4 cm/GW), the imaginary third-order susceptibility ($\text{Im } \chi^{(3)}$, -1.6×10^{-7} esu), and the figure of merit (FOM, 3.3×10^{-12} esu cm) at 515 nm are much larger than those at 1030 nm ($\alpha_{SA} = -82.9$ cm/GW, $\text{Im } \chi^{(3)} = -5.3 \times 10^{-10}$ esu, FOM = 3.4×10^{-14} esu cm). It is known that monolayer MoS₂ has a direct band gap (~ 1.9 eV), and multilayer MoS₂ has an indirect band gap (~ 1.2 eV).²⁷ When excited at 515 nm (per photon energy as 2.4 eV), both monolayer and multilayer MoS₂ can be excited with one photon, and when excited at 1030 nm (per photon energy as 1.2 eV), only multilayer MoS₂ can be excited with one photon while the monolayer being excited with two-photon absorption (TPA) (Fig. S3). TPA will result in a decrease of the transmission as opposed to the increase of the transmission for SA around the focal point in the Z-scan experiment.^{5,8} The ratio of the excited-state absorption cross section to ground-state absorption cross section (σ_{es}/σ_{gs}) are estimated to be 0.7 at 515 nm, and 0.5 at 1030 nm (Table S3), which is in consistent with the SA behavior of MoS₂ thin

film. The damage threshold for the fabricated MoS₂ thin films were ~ 400 nJ/pulse at 1030 nm, and ~ 40 nJ/pulse at 515 nm in our experiments, respectively. We also investigated the effect of film thickness on the NLO of fabricated MoS₂ thin films, and no obvious difference is observed. This is probably due to the similar thickness distribution for the nanosheets in films with different thicknesses even for the samples with different membrane pore sizes as shown in the absorption spectra and Raman spectra.

In addition, we compared the nonlinear response of the MoS₂ thin films with that of the MoS₂ dispersions in cyclohexyl pyrrolidinone (CHP) and the graphene filtered films with the film thickness as ~ 120 nm (Fig. 5b). The NLO parameters are shown in Table 1 (for a complete data, see Table S2 and S3). Obviously, the NLO performance of the MoS₂ thin films is much better than that of the MoS₂ dispersions with the Im $\chi^{(3)}$ and FOM at 515 nm are six and three orders of magnitude larger than that of the dispersions, respectively, and four and one order of magnitude larger than that of the dispersions at 1030 nm, respectively.⁸ Most importantly, the MoS₂ thin films exhibit better NLO performance than that of the graphene films, especially at 1030 nm. As shown in Table 1, the Im $\chi^{(3)}$ and FOM for MoS₂ thin film are about one order of magnitude larger at 515 nm, and about three times higher at 1030 nm, respectively, in compared to that of the graphene thin films. The α_{SA} of MoS₂ thin films was also larger than that of the graphene thin films at both 515 and 1030 nm, which is -82.9 cm GW⁻¹ for MoS₂ films and -76.4 cm GW⁻¹ for graphene thin films at 1030 nm. Overall, the layered MoS₂ neat films show high NLO performance in solid

state, better than that in liquid phase, and the graphene films. The high performance broadband ultrafast saturable absorption of the MoS₂ filtered thin films implying its potential applications in the field of nanophotonics, such as optical switching, mode-locking, beam shaping, super-resolution imaging, etc.^{5,8}

Conclusions

In this work, we have successfully obtained high quality MoS₂ thin films with controllable thicknesses, smooth surface and high optical homogeneity via vacuum filtration technique. The MoS₂ neat films show broadband ultrafast SA performance, which is better than that of the graphene films and the MoS₂ dispersions. Most importantly, the wafer-scale MoS₂ thin film is helpful in photonic fundamental studies and photonic devices applications, for it is large enough to satisfy laser spot size. Overall, this film fabrication technology affords a facile method for fabrication of layered MoS₂ optical films, which will greatly drive the potential application of 2D MoS₂ nanosheets in the field of nanophotonics. The method can also be applied to synthesize optical thin films with a wide range of nanomaterials, such as transition metal dichalcogenides, metal nanowires, carbon nanostructures, etc., from the corresponding exfoliated dispersions.

Acknowledgements

This work is supported in part by the National Natural Science Foundation of China (no. 61178007, no. 61308034, no. 51302285), Science and Technology Commission of Shanghai Municipality (no. 12ZR1451800, Nano Project no. 11nm0502400,

Shanghai Pujiang Program 12PJ1409400, and the Excellent Academic Leader of Shanghai no. 10XD1404600), the External Cooperation Program of BIC, CAS (No. 181231KYSB20130007), and Science Foundation Ireland (no. 12/IA/1306). J.W. thanks the National 10000-Talent Program and CAS 100-Talent Program for financial support. X.Y.Z. thanks Prof. Xiaoli Cui at Fudan University for the assistance on the TEM measurements.

References

1. Q. H. Wang, K. Kalantar-Zadeh, A. Kis, J. N. Coleman, and M. S. Strano, *Nat. Nanotechnol.*, 2012, **7**(11), 699-712.
2. J. N. Coleman, M. Lotya, A. O'Neill, S. D. Bergin, P. J. King, U. Khan, K. Young, A. Gaucher, S. De, R. J. Smith, I. V. Shvets, S. K. Arora, G. Stanton, H.-Y. Kim, K. Lee, G. T. Kim, G. S. Duesberg, T. Hallam, J. J. Boland, J. J. Wang, J. F. Donegan, J. C. Grunlan, G. Moriarty, A. Shmeliov, R. J. Nicholls, J. M. Perkins, E. M. Grievson, K. Theuwissen, D. W. McComb, P. D. Nellist, and V. Nicolosi, *Science*, 2011, **331**, 568-571.
3. S. Bertolazzi, J. Brivio, and A. Kis, *ACS Nano*, 2011, **5**, 9703-9709.
4. K. P. Loh, H. Zhang, W. Z. Chen, and W. Ji, *J. Phys. Chem. B.*, 2006, **110**, 1235-1239.
5. K. P. Wang, J. Wang, J. T. Fan, M. Lotya, A. O'Neil, D. Fox, Y. Y. Feng, X. Y. Zhang, B. X. Jiang, Q. Z. Zhao, H. Z. Zhang, J. N. Coleman, L. Zhang, and W. J. Blau, *ACS Nano*, 2013, **7**(10), 9260-9267.
6. H. Zhang, S. B. Lu, J. Zheng, J. Du, S. C. Wen, D. Y. Tang, and K. P. Loh, *Opt. Express*, 2014, **22**(6), 7249-7260.

-
7. H. Liu, A.-P. Luo, F.-Z. Wang, R. Tang, M. Liu, Z.-C. Luo, W.-C. Xu, C.-J. Zhao, and H. Zhang, *Opt. Lett.*, 2014, **39**(15), 4591-4594.
 8. K. P. Wang, Y. Y. Feng, C. X. Chang, J. X. Zhan, C. W. Wang, Q. Z. Zhao, J. N. Coleman, L. Zhang, W. J. Blau, and J. Wang, *Nanoscale*, 2014, **6**, 10530-10535.
 9. J. Du, Q. K. Wang, G. B. Jiang, C. W. Xu, C. J. Zhao, Y. J. Xiang, Y. Chen, S. C. Wen, and H. Zhang, *Scientific Reports*, 2014, **4**, 6346.
 10. Y. Z. Huang, Z. Q. Luo, Y. Y. Li, M. Zhong, B. Xu, K. J. Che, H. Y. Xu, Z. P. Cai, J. Peng, and J. Weng, *Opt. Express*, 2014, **22**(21), 25258-25266.
 11. Z. Q. Luo, Y. Z. Huang, M. Zhong, Y. Y. Li, J. Y. Wu, B. Xu, H. Y. Xu, Z. P. Cai, J. Peng, and J. Weng, *J. Lightwave Technology*, 2014, **32**(24), 4679-4686.
 12. J. Wang and W. J. Blau, *J. Optics A - Pure and Applied Optics*, 2009, **11**, 024001.
 13. L. Polavarapu, N. Venkatram, W. Ji, and Q. H. Xu, *ACS Appl. Mater. Interfaces*, 2009, **1**, 2298-2303.
 14. X. Cheng, N. N. Dong, B. Li, X. Y. Zhang, S. F. Zhang, J. Jiao, W. J. Blau, L. Zhang, and J. Wang, *Opt. Express*, 2013, **21** (14), 16486-16493.
 15. Z. P. Guan, L. Polavarapu, and Q.-H. Xu, *Langmuir*, 2010, **26**, 18020-18023.
 16. K. S. Novoselov, D. Jiang, F. Schedin, T. J. Booth, V. V. Khotkevich, S. V. Morozov, and A. K. Geim, *Proc. Natl. Acad. Sci. U.S.A.*, 2005, **102**, 10451-10453.
 17. Y. H. Lee, X. Q. Zhang, W. Zhang, M. T. Chang, C. T. Lin, K. D. Chang, Y. C. Yu, J. T. W. Wang, C. S. Chang, L.-J. Li, and T.W. Lin, *Adv. Mater.*, 2012, **24**, 2320-2325.
 18. X. Wang, H. Feng, Y. Wu, and L. Jiao, *J. Amer. Chem. Soc.*, 2013, **135**, 5304-5307.

-
19. X. Ling, Y.-H. Lee, Y. X. Lin, W. J. Fang, L. L. Yu, M. S. Dresselhaus, and J. Kong, *Nano Lett.*, 2014, **14** (2), 464-472.
 20. G. Eda, G. Fanchini, and M. Chhowalla, *Nat. Nanotechnol.*, 2008, **3**, 270-274.
 21. M. Lotya, P. J. King, U. Khan, S. De, and J. N. Coleman, *ACS Nano*, 2010, **4** (6), 3155-3162.
 22. S. De, P. J. King, M. Lotya, A. O'Neill, E. M. Doherty, Y. Hernandez, G. S. Duesberg, and J. N. Coleman, *Small*, 2010, **6**(3) 458-464.
 23. S. X. Wang, H. H. Yu, H. J. Zhang, A. Z. Wang, M. W. Zhao, Y. X. Chen, L. M. Mei, and J. Y. Wang, *Adv. Mater.*, 2014, **26**, 3538-3544.
 24. J. Wang, Y. Hernandez, M. Lotya, J. N. Coleman, and W. J. Blau, *Adv. Mater.*, 2009, **21**, 2430-2435.
 25. R. J. Smith, P. J. King, M. Lotya, C. Wirtz, U. Khan, S. De, A. O'Neill, G. S. Duesberg, J. C. Grunlan, G. Moriarty, J. Chen, J. Z. Wang, A. I. Minett, V. Nicolosi, and J. N. Coleman, *Adv. Mater.*, 2011, **23**, 3944-3948.
 26. G. Cunningham, M. Lotya, C. S. Cucinotta, S. Sanvito, S. D. Bergin, R. Menzel, M. S. Shaffer, and J. N. Coleman, *ACS Nano*, 2012, **6**, 3468-3480.
 27. K. F. Mak, C. Lee, J. Hone, J. Shan, and T. F. Heinz, *Phys. Rev. Lett.*, 2010, **105**(13), 136805.
 28. G. Eda, H. Yamaguchi, D. Voiry, T. Fujita, M. Chen, and M. Chhowalla, *Nano Lett.*, 2011, **11**(12), 5111-5116.
 29. Y. Lee, J. Lee, H. Bark, I.-K. Oh, G. H. Ryu, Z. Lee, H. Kim, J. H. Cho, J.-H. Ahn, and C. Lee, *Nanoscale*, 2014, **6**(5), 2821-2826.
 30. C. Lee, H. Yan, L. E. Brus, T. F. Heinz, J. Hone, and S. Ryu, *ACS Nano*, 2010, **4**, 2695-2700.
 31. A. O'Neill, U. Khan, and J. N. Coleman, *Chem. Mater.*, 2012, **24**, 2414-2421.

-
32. M. Pokrass, Z. Burshtein, R. Gvishi, and M. Nathan, *Optical Mater. Express*, 2012, **2**(6), 825-838.
 33. T. Korn, S. Heydrich, M. Hirmer, J. Schmutzler, and C. Schuller, *Appl. Phys. Lett.*, 2011, **99**, 102109.
 34. R. Wang, B. A. Ruzicka, N. Kumar, M. Z. Bellus, H.-Y. Chiu, and H. Zhao, *Phys. Rev. B.*, 2012, **86**, 045406.
 35. W. J. Cao, H. Y. Wang, A. P. Luo, Z. C. Luo, and W. C. Xu, *Laser Phys. Lett.*, 2012, **9**, 54.

Figure 1

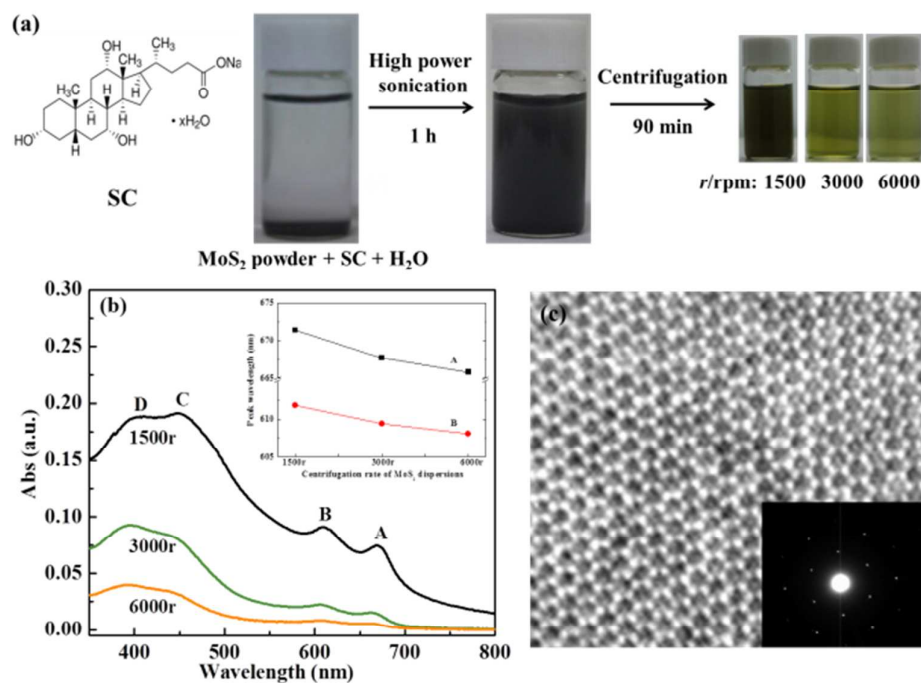


Fig. 1 (a) Preparation process for MoS₂ dispersions by liquid-phase exfoliation method. (b) Absorption spectra of MoS₂ dispersions prepared via different centrifugation rate. Inset: Profiles for the A and B excitonic transition absorption along with increasing of centrifugation rates. (c) HRTEM image of MoS₂ nanosheets from dispersion with a centrifugation rate of 3000 rpm. Inset: electron diffraction pattern in (c).

Figure 2

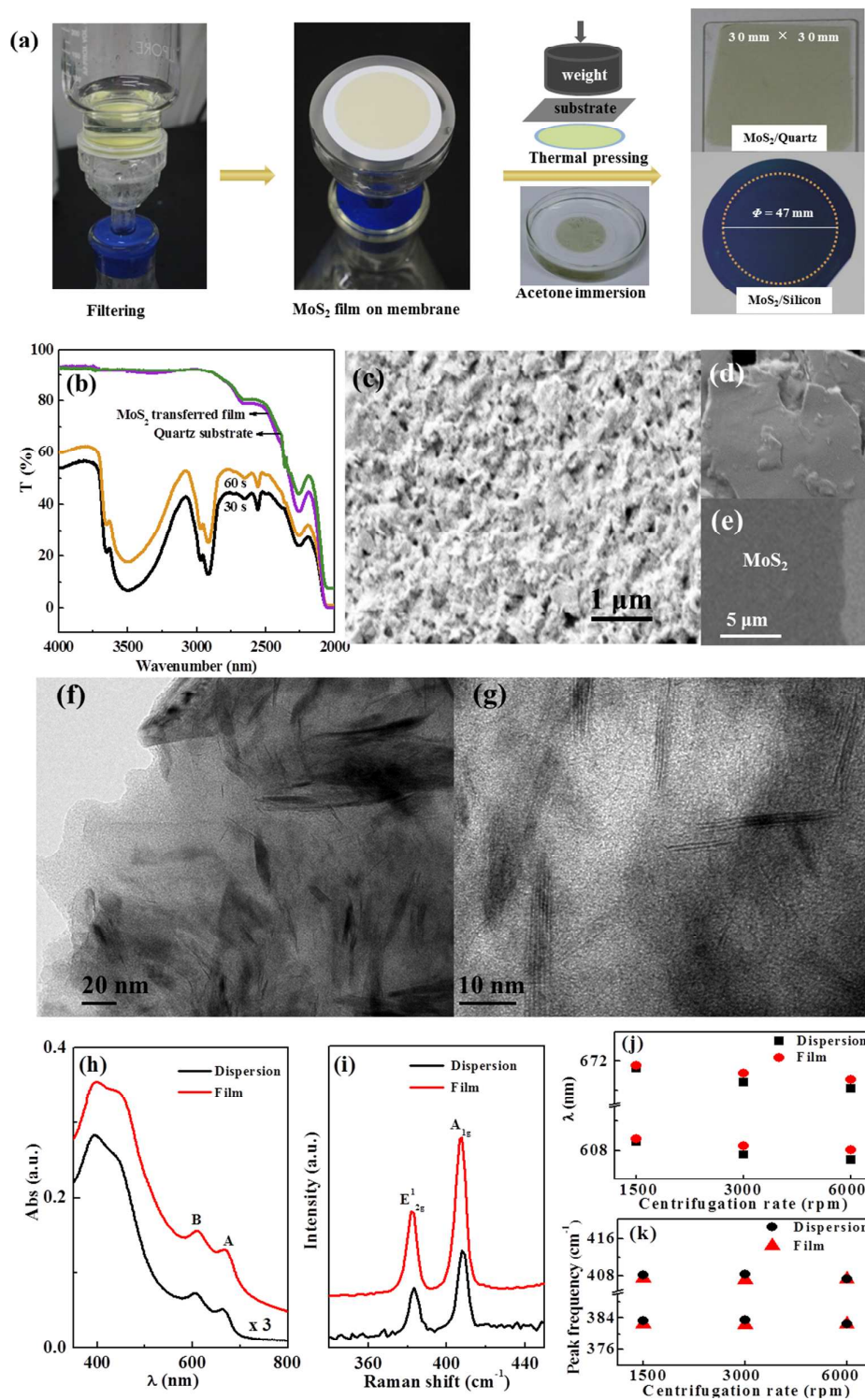


Fig. 2 (a) Fabrication process for transferred MoS₂ films. The process includes three

steps: vacuum filtration, thermal pressing, and acetone immersion. (b) FTIR spectra of quartz/MoS₂/membrane films immersed in acetone with 30 s, 60 s, and 3 h in compared to the pure quartz substrate. (c) FE-SEM image of MoS₂ filtered film on nitrocellulose membrane with pore size of 100 nm from 4 mL of MoS₂ dispersions at a centrifugation rate of 3000 rpm. (d) High resolution FE-SEM image of MoS₂ flakes in (c). (e) Low resolution FE-SEM image of transferred MoS₂ film on quartz substrate. (f,g) HRTEM images of MoS₂ filtered films. The sample for HRTEM was fabricated by scrubbing off MoS₂ from the substrate followed by dispersing in absolute alcohol, and then dropped onto copper grid. (h) Comparative absorption spectra of MoS₂ neat films and dispersions at 3000 rpm. (i) Comparative Raman spectra of MoS₂ neat films and dispersions at 3000 rpm. (j) Wavelengths of A and B excitonic transition absorption for films and dispersions along with increasing of centrifugation rates. (k) Frequencies of E_{2g}¹ and A_{1g} Raman modes for films and dispersions along with increasing of centrifugation rates. The films are fabricated using membranes with pore size of 100 nm.

Figure 3

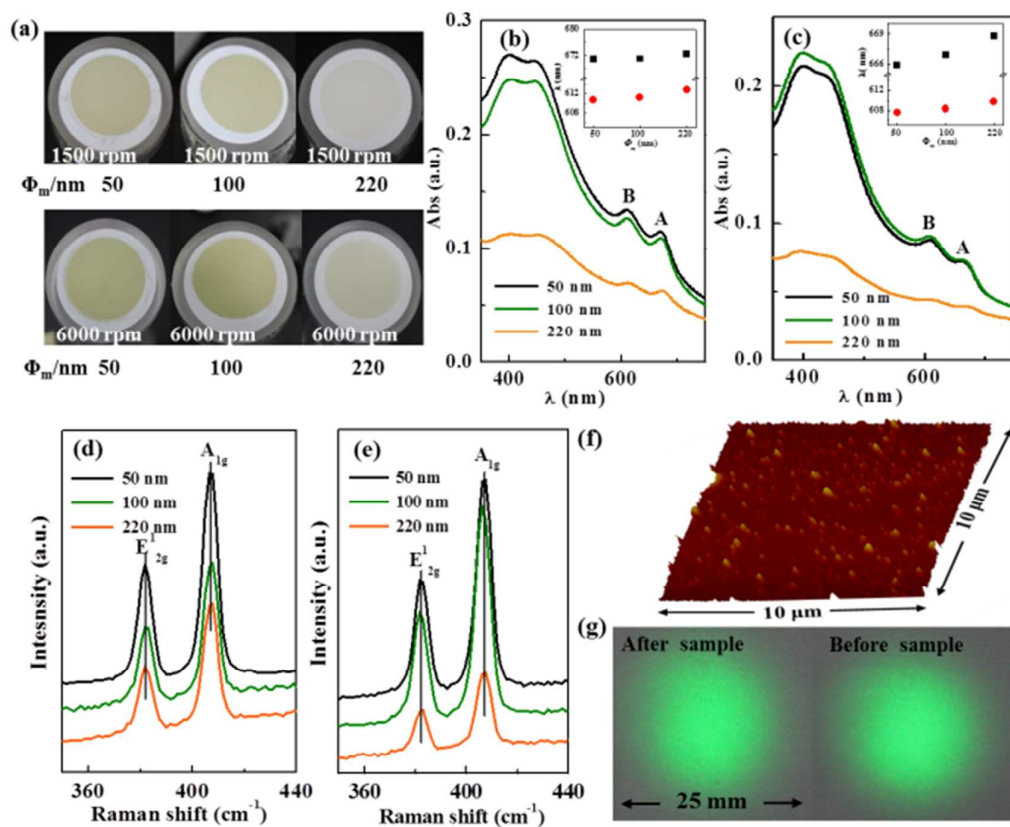


Fig. 3 Effect of membrane pore size. (a) Photographs of untransferred MoS₂ filtered films with different membrane pore sizes. (b-c) Absorption spectra and (d-e) Raman spectra of MoS₂ films with different membrane pore sizes from dispersions at 1500 and 6000 rpm, respectively. Inset: Profiles for the A and B excitonic transition absorption along with increasing of membrane pore size. (f) Typical AFM image of the surface of MoS₂ thin film on quartz substrate. (g) Photograph of a collimated beam before and after passing through MoS₂ thin films (532 nm, CW laser).

Figure 4

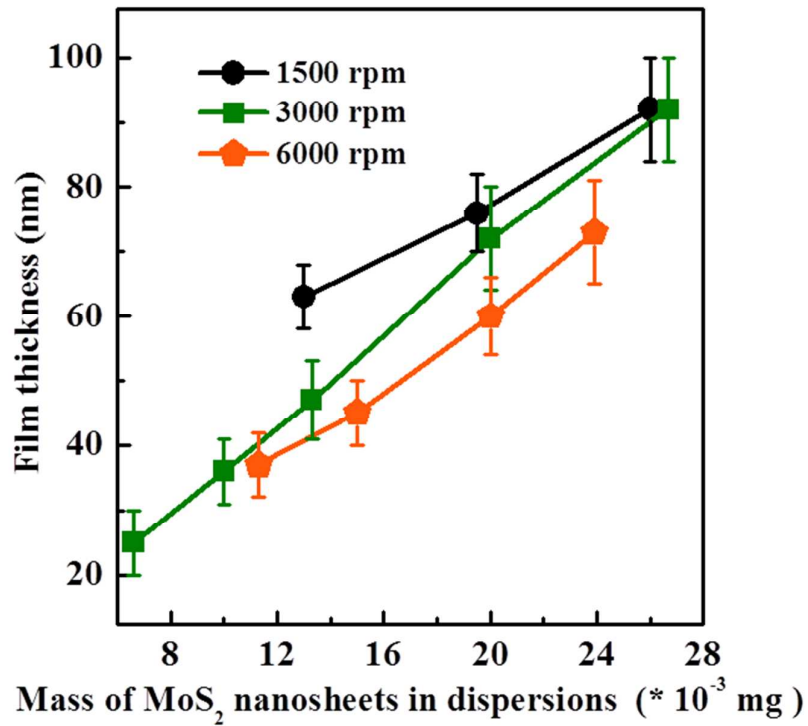


Fig. 4 Relationship between film thickness and amounts of MoS₂ nanosheets in dispersions with different centrifugation rates. The mass of MoS₂ flakes is obtained from $C * V$, where C is the concentration of dispersions, V is the dispersion volume.

Figure 5

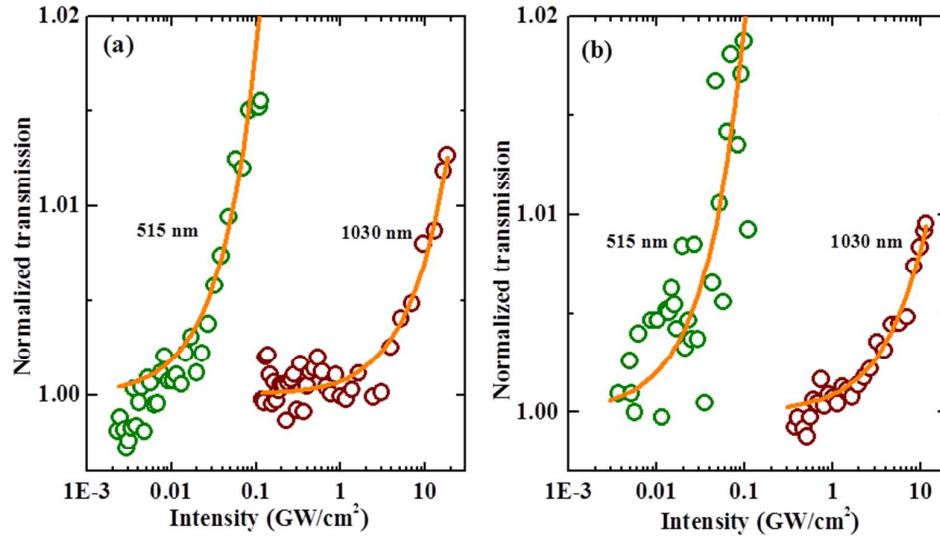


Fig. 5 Normalized transmission as a function of input laser intensity for (a) MoS₂ thin film and (b) graphene thin film. The solid lines are the theoretical fit curves by a slow saturable absorber model.

Table 1 Linear and NLO parameters of the transferred MoS₂ neat films in compared to those of MoS₂ dispersions and graphene filtered films.

Sample	Laser	T [%]	α_{SA} [cm GW ⁻¹]	I_s [GW cm ⁻²]	$\text{Im}\chi^{(3)}$ [esu]	FOM [esu cm]	σ_{gs} [cm ²]	σ_{es} [cm ²]
MoS ₂ film	515 nm	65.0	-2.1×10 ⁴	2.2	-1.6×10 ⁻⁷	3.3×10 ⁻¹²	4.7×10 ⁻¹⁵	2.0×10 ⁻¹⁵
	1030 nm	87.0	-82.9	171	-5.3×10 ⁻¹⁰	3.4×10 ⁻¹⁴	2.9×10 ⁻¹⁷	1.5×10 ⁻¹⁷
MoS ₂ in CHP ^{a)}	515 nm	7.9	-0.36	58	-1.3×10 ⁻¹³	5.1×10 ⁻¹⁵	/	/
	1030 nm	30.9	-9.2×10 ⁻²	114	-6.7×10 ⁻¹⁴	5.7×10 ⁻¹⁵	/	/
Graphe-ne film	515 nm	64.6	-2.0×10 ⁴	1.5	-2.2×10 ⁻⁸	6.1×10 ⁻¹³	3.3×10 ⁻¹⁵	6.4×10 ⁻¹⁶
	1030 nm	83.0	-76.4	192	-1.7×10 ⁻¹⁰	1.0×10 ⁻¹⁴	4.0×10 ⁻¹⁷	2.8×10 ⁻¹⁷

^{a)} MoS₂ dispersions in CHP were obtained by liquid-phase exfoliation method. [8]